Metal-organic Frameworks Derived CoS$_2$-Co/N-doped Porous Carbon with Extremely High Electrocatalytic Stability for the Oxygen Reduction Reaction

Xin Gu[1], Ying Wang[1], Liting Yan[1], Liangjun Li[1], Pengcheng Dai[1,], Hongbo Wang[2,*], Xuebo Zhao[1,3,*]*

[1] Institute of Unconventional Petroleum and Renewable Energy, China University of Petroleum (East China), Qingdao, 266580, P. R. China.
[2] Key Laboratory of Optoelectronic Chemical Materials and Devices, Ministry of Education, School of Chemical and Environmental Engineering, Jianghan University, Wuhan, 430056, P. R.China.
[3] State Key Laboratory of Heavy Oil Processing, China University of Petroleum (East China), Qingdao, 266580, P. R. China.
[*]E-mail: dpcapple@upc.edu.cn, hongbo.wang@csu.edu.cn, zhaoxuebo@upc.edu.cn

The electrocatalytic performances for the oxygen reduction reaction (ORR) highly depend on the structure and composition of catalysts. In this work, a novel non-precious metal catalyst (CoS$_2$-Co/N-doped porous carbon) has been fabricated by the carbonization of metal-organic frameworks (MOFs) with a consequent sulfuration process. The resultant nanocomposite exhibits highly desirable structure features for ORR, such as high-efficient Co-N-C active sites, porous carbon nanostructures for rapid mass transfer, and CoS$_2$ protective layers that prevent Co-N-C active sites from deactivation. As a result, the rationally designed catalyst shows extremely high electrocatalytic stability with a high current retention of ~ 98 % after 10 h in alkaline media.

1. INTRODUCTION

The electrocatalytic oxygen reduction reaction (ORR) has been a rate-determining step in all kinds of energy storage or conversion systems, mainly including metal-air batteries and fuel cells.[1-3] Developing highly durable and active catalysts for sluggish ORR is greatly important for the practical application of these devices. So far, Pt-based catalysts have exhibited the highest ORR activity in alkaline media.[4, 5] However, the poor durablity, undesirable crossover effect, as well as the high cost and scarcity of Pt resources, have hampered their practical applications.[6]

To replace the conventional Pt-based catalysts, various non-precious metal or metal-free catalysts, including transition metal-nitrogen-carbon (M-N-C, M=Fe, Co, Ni) materials,[7-9] metal oxides or chalcogenides loaded on carbon nanostructures,[10-12] and heteroatoms doped carbon materials,[13-17] have been developed. Among them, M-N-C with active sites of surface nitrogen coordinated metals exhibits the best electrocatalytic activity.[18] In general, M-N-C is synthesized by carbonizing organic molecules/polymers and transition metal ions, due to its simple operation and easy scale-up.[8, 19, 20] However, this strategy does not allow precise controls on the size, shape, and structure of organic-inorganic precursors, which generates nonuniform distribution of the active cites, and thus leads to the low catalytic activity. Recently, metal-organic frameworks (MOFs), a type of porous crystalline materials, have been explored as novel precursors and templates to prepare efficient M-N-C catalysts.[9, 21] The M-N-C catalysts derived from MOFs have two main advantages: (i) MOFs derived porous carbon structures can effectively enhance the contact between active sites and electrolyte, and promote the mass transport for ORR; (ii) uniformly distributed active sites further enhance the electrocatalytic activity for ORR. Moreover, other ORR-active compounds (e.g. metal oxides, metal sulfides and graphitic carbons) have been introduced into M-N-C structures to further improve the electrocatalytic performances for ORR.[8, 22-24] For example, Shuhong Yu *et al.* reported that the introduce of graphitic carbon in Fe-N-C nanofibers exhibited comparable electrocatalytic activity to 20 wt. % Pt/C catalyst in alkaline media, which is among the best non-precious metal catalysts.[8] Xiongwen (David) Lou *et al.* also reported that the introduction of Co_8S_9 shells remarkably improved the electrocatalytic stability of Co-N-C nanostructures. The Co_8S_9 shells could prevent the Co-N-C catalyst from deactivation.[23]

Herein, we report a new type of non-precious metal catalyst based on CoS_2-Co nanoparticles loaded on N-doped porous carbon nanostructures, which are prepared by the carbonization of MOFs with a consequent sulfuration process. Such a unique catalyst exhibits desirable structure features for ORR, such as high-efficient intrinsic active sites (Co-N-C), porous carbon nanostructures for rapid mass transfer, and CoS_2 shells that can prevent highly active Co-N-C from deactivation. The rationally designed electrocatalyst shows excellent ORR activity and stability in alkaline media.

2. EXPERIMENTAL

2.1 Synthesis of ZIF-67 precursors

For the synthesis of ZIF-67 precursors, cobalt nitrate hexahydrate (20 mmol) and 2-methylimidazole (80 mmol) were each dissolved in 200 mL of methanol. Then, the two solutions were mixed rapidly and aged for 24 h at room temperature. Finally, the precipitate was obtained by filtration, washed with methanol for several times, and dried under vacuum at 100 ^{o}C.

2.2 Synthesis of CoS₂-Co/NC nanocomposites

The as-prepared ZIF-67 precursors were firstly converted to Co/NC nanocomposites by the heat treatment at 600 ^{o}C for 2 h in Ar flow. Subsequently, the obtained Co/NC (240 mg) was grinded

with thiourea (912 mg) thoroughly, and then the resultant mixture was subjected to sulfuration at 180 °C for 24 h in a N_2 filled Teflon-lined autoclave (50 mL). The final products, CoS_2-Co/NC nanocomposites, were obtained by washing with ethanol, and drying under vacuum.

2.3 Structure characterization

Powder XRD patterns were obtained on a Bruker D8 advanced X-ray diffractometer, using Ni-filtered Cu-Kα line as radiation source. FESEM images and EDS specturm were recorded by a JSM 6700F field emission scanning electron microscope. TEM images were achieved on a JEM 1011 transmission electron microscope. Raman spectra were acquired from a NEXUS 670 Raman spectrometer using an excitation wavelength of 632 nm. XPS patterns were collected on an X-ray photoelectron spectrometer (ESCALAB 250, USA) to identify the surface chemical state and composition. N_2 sorption measurement was performed on a Quadrasorb SI analyzer at 77K. Brunauer-Emmett-Teller (BET) analysis was performed to determine the surface area.

2.4 Electrochemical measurements

The electrocatalytic activity of the catalysts (CoS_2-Co/NC, Co/NC, commercial 10 wt. % Pt/C) was examined by an electrochemical workstation (CHI760E, China) and a RRDE apparatus (ATA-1B, China) with a three-electrode cell system. A polished glassy carbon rotating disk electrode (RDE, d = 3 mm) was used as a support. The catalyst suspension was prepared by dispersing 2 mg of the catalyst in 1 mL of 0.5 wt. % nafion ethanol/H_2O (volume ratio, 1:1) solution under sonication for 30 min. 4 μL of the suspension was dropped onto the polished RDE for electrocatalytic oxygen reduction. An Ag/AgCl (sat. KCl) electrode and a Pt plate were applied as reference electrode and counter electrode. All potentials reported herein were referenced to the reversible hydrogen electrode (RHE) with the following equation:

$$E(\text{RHE}) = E(\text{Ag/AgCl}) + 0.965$$

The cyclic voltammetry (CV) measurements for CoS_2-Co/NC, Co/NC and 10 wt. % Pt/C in both N_2- and O_2-saturated 0.1 M KOH solutions were performed at a scan rate of 100 mV s^{-1}. The polarization curves for ORR were conducted at various rotation speeds from 225 to 1600 rpm with a scan rate of 50 mV s^{-1}. The current-time (i-t) curves were tested in O_2-saturated 0.1 M KOH electrolyte under a fixed potential of 0.5 V (vs. RHE) at the rotation speed of 1600 rpm. Before testing, the electrode was cycled at 100 mV s^{-1} until reproducible CV curves were obtained. On the basis of RDE data, the electron transfer number (n) was calculated from Koutecky-Levich (K-L) equation:

$$1/j = 1/j_k + 1/B\omega^{1/2}$$

where j and j_k are the measured current density and kinetic-limiting current density, and ω represents the rotation speed. B can be determined from the slope of K-L plots. The electron number (n) can be obtained from the following equation:

$$n = B/(0.2F(D_{O2})^{2/3}(v)^{-1/6}C_{O2})$$

where F is Faraday constant (96485 C mol^{-1}), D_{O2} is the diffusion coefficient of O$_2$ (1.9×10^{-5} cm^2 s^{-1}), v is the kinetic viscosity (v = 0.01 cm^2 s^{-1}) and C_{O2} is the bulk concentration of O$_2$ (1.2×10^{-6} mol cm^{-3}). When expressing the rotation speed in rpm, the constant 0.2 is applied.

3. RESULTS AND DISCUSSION

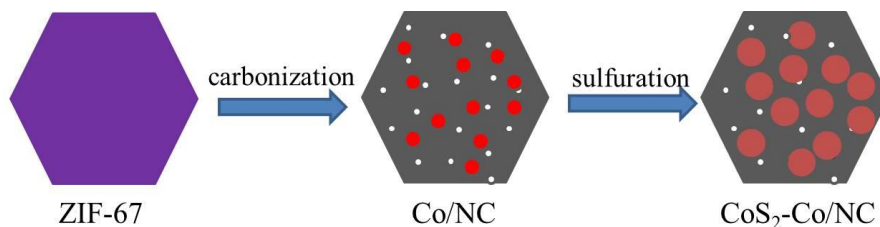**Figure 1.** Schematic illustration on the synthesis process for CoS$_2$-Co/N-doped porous carbon.

The synthetic process for CoS$_2$-Co/N-doped porous carbon (CoS$_2$-Co/NC) is illustrated in Fig. 1. Firstly, Co-based Zeolitic Imidazolate Frameworks (ZIF-67) were prepared by a precipitation method in methanol solution at room temperature, using cobalt salt and 2-methylimidazole as reactants. Then, the as-obtained ZIF-67 precursors were transferred to a tube furnance, followed by heat-treatment in the atmosphere of Ar. In this process, Co/N-doped porous carbon nanocomposites (Co/NC) were formed. Finally, CoS$_2$-Co/NC nanocomposites were achieved by the sulfidation reaction between Co/NC and thiourea in N$_2$ protection.
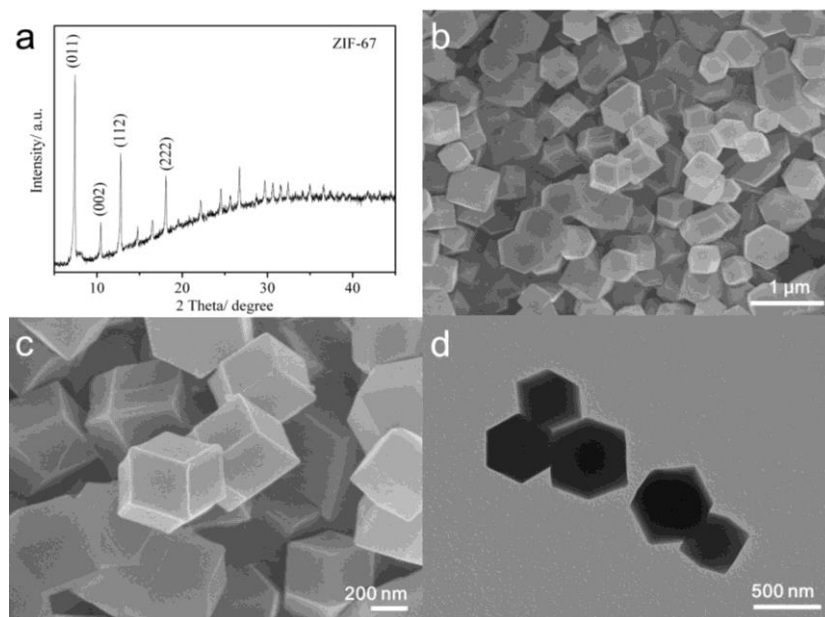

Figure 2. (a) XRD pattern, (b, c) FESEM images and (d) TEM image of ZIF-67 precursors.
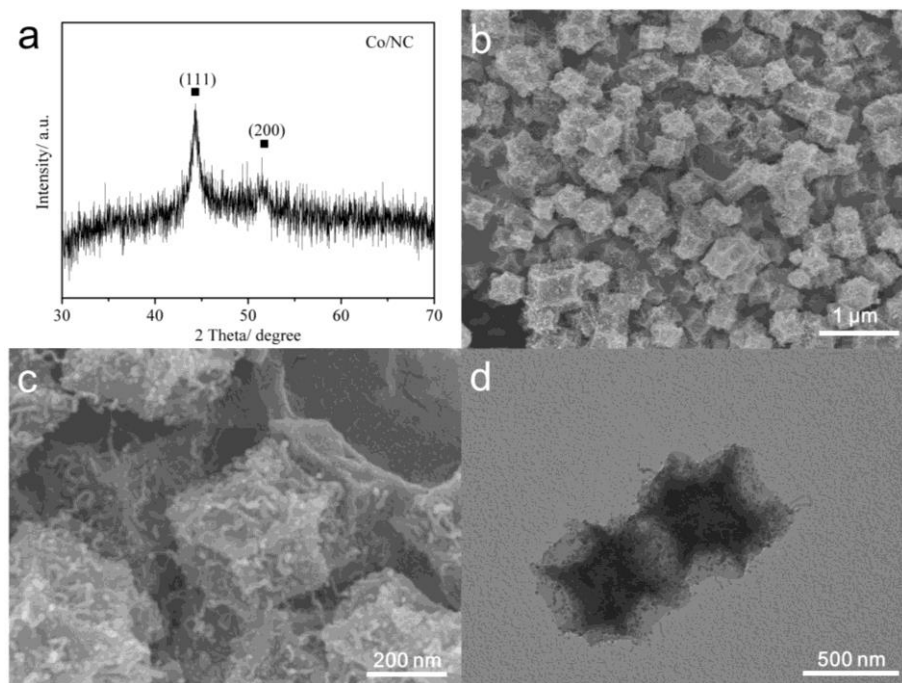
Figure 3. (a) XRD pattern, (b, c) FESEM images and (d) TEM image of Co/NC nanocomposites.
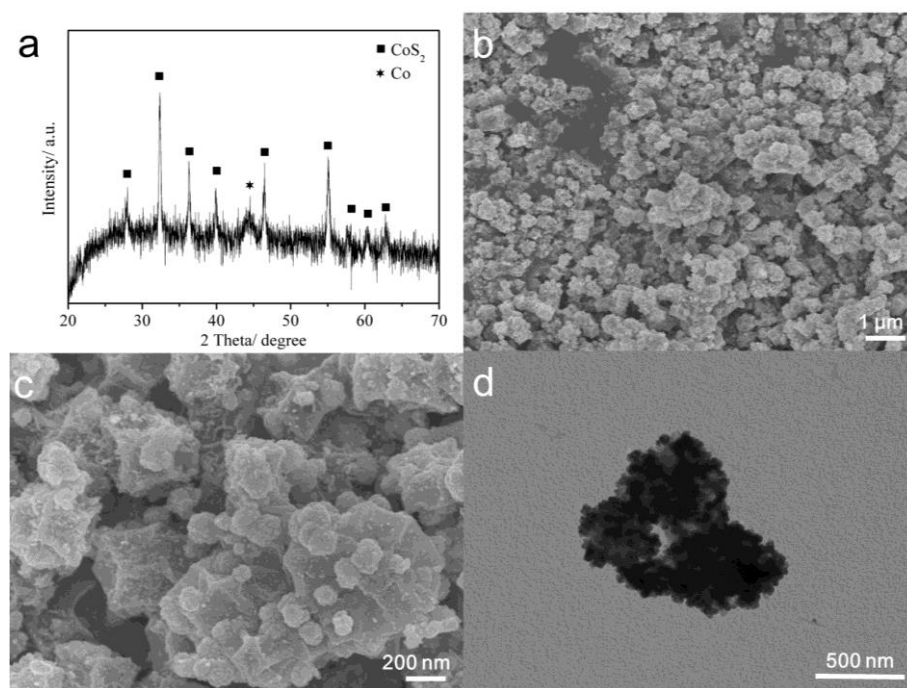

Figure 4. (a) XRD pattern, (b, c) FESEM images and (d) TEM image of CoS$_2$-Co/NC nanocomposites.

The structures of the products obtained at different stages of the synthetic process were characterized by XRD, FESEM and TEM measurements. As shown in Fig. 2a, XRD pattern of ZIF-67 precursors shows typical diffraction peaks from (011), (002), (112) and (222) planes, being well consistent with previous reports.[9, 23] The FESEM and TEM images of the pre-prepared ZIF-67

precursors are presented in Fig. 2b-d, where the polyhedral morphology with smooth surface dominates this product. These ZIF-67 polyhedrons have an average size of ~ 500 nm. High-temperature annealing of these precursors resulted in the formation of cubic-phase Co (JCPDS Card, No 15-0806), as described in Fig. 3a. FESEM and TEM images (Fig. 3b-d) indicate that Co nanoparticles are encapsulated in carbon and the resultant Co/NC nanocomposites inherit the polyhedral morphology but with rough surface.
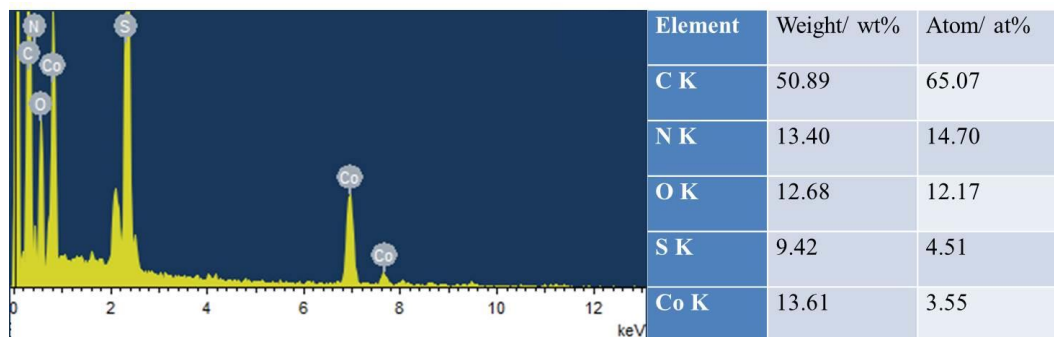
Element	Weight/ wt%	Atom/ at%
C K	50.89	65.07
N K	13.40	14.70
O K	12.68	12.17
S K	9.42	4.51
Co K	13.61	3.55

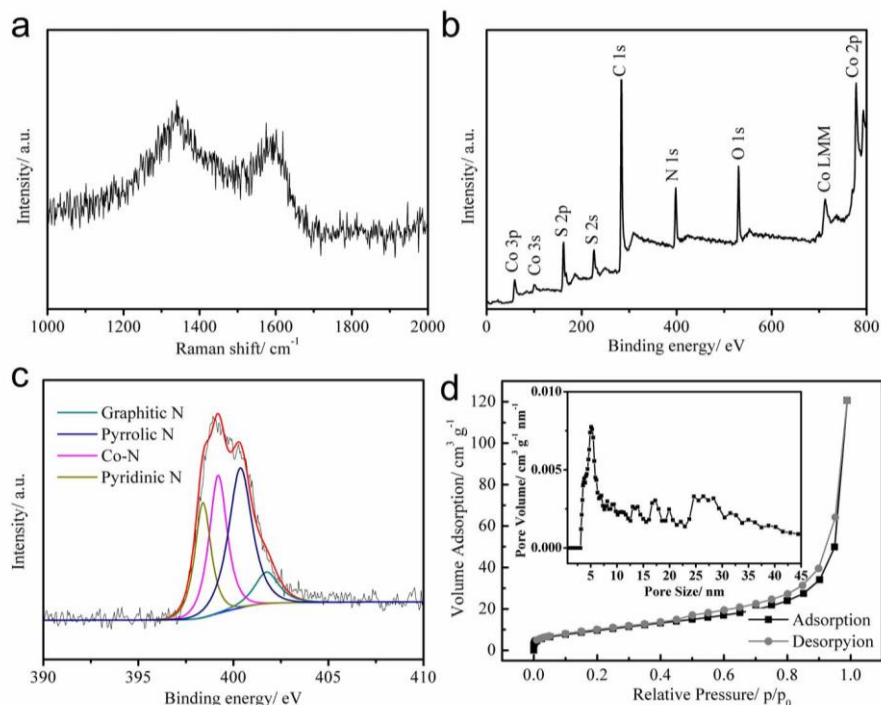**Figure 5.** Energy dispersive spectroscopy (EDS) of CoS_2-Co/NC nanocomposites.

Figure 6. (a) Raman spectrum of CoS_2-Co/NC; (b) XPS survey spectrum for CoS_2-Co/NC; (c) High resolution N 1s XPS spectrum for CoS_2-Co/NC; (d) Nitrogen adsorption-desorption isotherm and pore-size-distribution curve of CoS_2-Co/NC.

After a sulfidation process, metallic Co nanoparticles were partially transformed to CoS_2 (JCPDS Card, No 41-1471, Fig. 4a), and the encapsulation configuration was destroyed due to the larger particle size of CoS_2-Co than Co (Fig. 4b-d). The energy dispersive spectrum (Fig. 5) indicates that CoS_2-Co/NC nanocomposite is mainly consisted of C (50.89 wt. %), N (13.40 wt. %), O (12.68

wt. %), S (9.42 wt. %) and Co (13.61 wt. %) elements. And the atomic ratio of Co/S is calculated to be about 1/1.27, indicating the co-existence of Co and CoS_2 in this product, which agrees well with the XRD result.

As presented in Fig. 6a, Raman spectrum indicates the presence of carbon in CoS_2-Co/NC nanocomposites. Two peaks at 1342 and 1591 cm^{-1} are attributed to the D and G bands of carbon. X-ray photoelectron spectra (XPS) were obtained to clarify the surface chemical state and composition of CoS_2-Co/NC nanocomposites. The survey XPS spectrum (Fig. 6b) further confirms the presence of C, N, O, S and Co elements in the product. The atomic ratio of Co/S calculated from XPS data is about 1/2, which conflicts with that from EDS data, suggesting that the CoS_2-Co/NC nanocomposite is comprised of outer CoS_2 and inner Co. The surface doping of nitrogen in carbon is calculated as 15.5 at. %. The high resolution XPS spectrum for N 1s (Fig. 6c) can be fitted to four peaks centered at 398.4, 399.2, 400.4 and 401.7 eV, belonging to pyridinic N (22.2 %), Co-N (29.7 %), pyrrolic N (39.0 %) and graphitic N (9.1 %), respectively.[24, 25] The high content of surface nitrogen coordinated Co active sites would facilitate this nanocomposite to achieve high ORR activity. The pore structure in the CoS_2-Co/NC nanocomposite was characterized by N_2 sorption at 77 K. As presented in Fig. 6d, the nitrogen sorption isotherms give an obvious hysteresis loop, indicating the mesoporous structures in the composite. The average pore size is approximately 5.1 nm by the NLDFT method, and the BET surface area is determined to be about 35.6 $m^2 \, g^{-1}$. The as-obtained mesoporous structures can effectively enhance the contact areas between electrode and electrolyte, promote the mass transport of ORR, and thus improve the ORR performances.
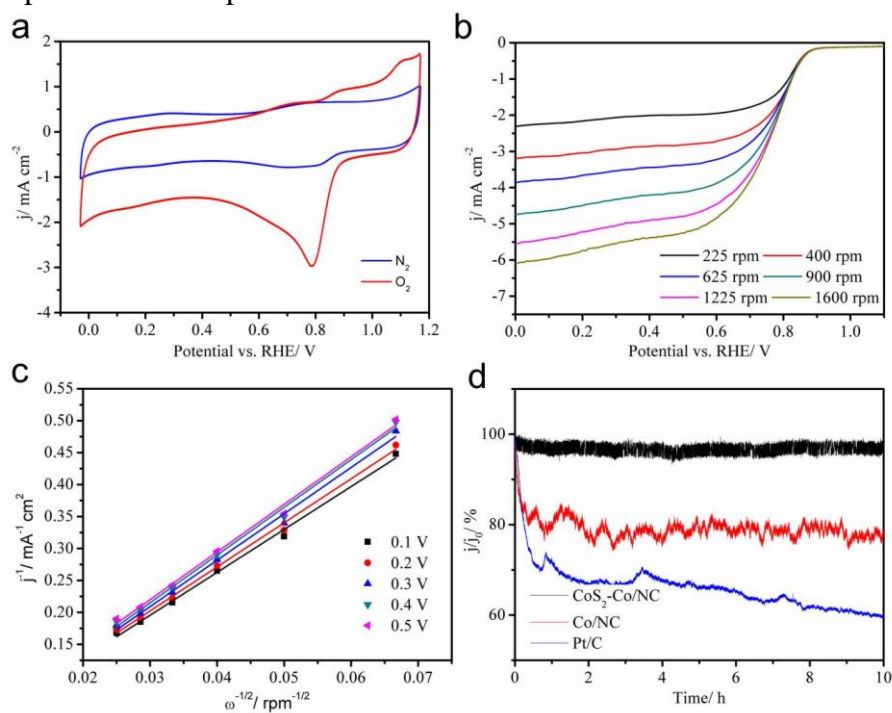

Figure 7. (a) CV curves of CoS_2-Co/NC catalyst in N_2- and O_2-saturated 0.1 M KOH electrolyte at a scan rate of 100 mV s^{-1}, (b) LSV curves of CoS_2-Co/NC catalyst at different rotation rates at a scan rate of 50 mV s^{-1}, (c) Koutecky–Levich plots of CoS_2-Co/NC catalyst at various potentials, (d) Stability evaluation of CoS_2-Co/NC, Co/NC and commercial 10 wt. % Pt/C catalysts at 0.5 V in O_2-saturated 0.1 M KOH electrolyte at 1600 rpm.

The electrocatalytic activity of CoS_2-Co/NC nanocomposites towards ORR was examined by cyclic voltammetry measurements conducted in N_2- or O_2-saturated 0.1 M KOH electrolyte at a scanning rate of 100 mV s^{-1}. A well-defined cathodic peak at about 0.79 V (vs. RHE) is observed for CoS_2-Co/NC catalyst in O_2-saturated 0.1 M KOH electrolyte in Fig. 7a, whereas featureless slope is presented in N_2-saturated 0.1 M KOH electrolyte. The onset potential is determined to be about 0.89 V (vs. RHE). Both the cathodic peak potential and onset potential of CoS_2-Co/NC catalyst are very close to those of Co/NC catalyst (Fig. 8), suggesting that the introduction of CoS_2 shells does not lower the electrocatalytic activity of Co-N-C structures. Moreover, the cathodic peak potential and onset potential of CoS_2-Co/NC catalyst are comparable to those of commercial 10 wt. % Pt/C (Fig. 8), suggesting a superior ORR electrocatalytic activity for CoS_2-Co/NC nanocomposites in alkaline electrolyte.
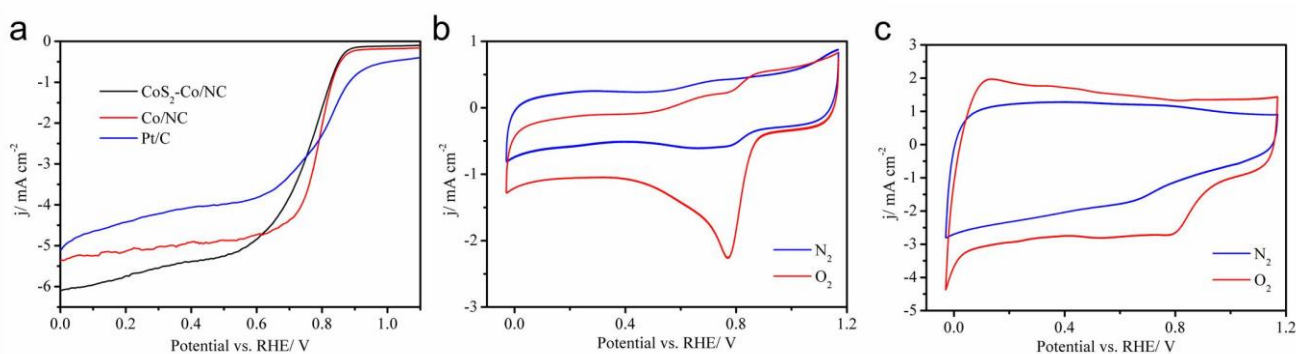

Figure 8. (a) Comparison of the LSV curves of CoS_2-Co/NC, Co/NC and commercial 10 wt. % Pt/C catalysts at the rotation speed of 1600 rpm, (b) CV curves of Co/NC catalyst in N_2- and O_2-saturated 0.1 M KOH electrolyte at a scan rate of 100 mV s^{-1}, (c) CV curves of a commercial 10 wt. % Pt/C catalyst in N_2- and O_2-saturated 0.1 M KOH electrolyte at a scan rate of 100 mV s^{-1}.

To further evaluate the ORR reaction on CoS_2-Co/NC catalyst, linear sweep voltammograms (LSVs) were recorded on a rotating disk electrode (RDE) at various rotating rates of 225-1600 rpm in O_2-saturated 0.1 M KOH electrolyte at a scanning rate of 50 mV s^{-1}. As presented in Fig. 7b, the polarization curves show a sharp increase of current densities, and then the current density increases slowly with the negative shift of potential, which is typical for porous electrocatalysts (Fig. 6d).[14] The limiting current density at the rotating speed of 1600 rpm reaches 5.3 mA cm^{-2} at 0.5 V (vs. RHE), which is superior to Co/NC (4.9 mA cm^{-2}) and commercial 10 wt. % Pt/C (4.0 mA cm^{-2}) under the same conditions (Fig. 8a). Fig. 7c displays the corresponding Koutecky-Levich (K-L) plots where good linearity in a wide potential range from 0.1 to 0.5 V can be observed, which is indicative of first-order reaction kinetics for ORR with respect to dissolved oxygen concentration. The average value of electron transfer number (n) at 0.1-0.5 V is calculated to be about 3.9, approximate to the theoretical value of Pt/C catalyst (n=4.0), indicating a near four-electron ORR process for CoS_2-Co/NC catalyst in alkaline medium.

As the durability is very important for the practical applications of ORR catalysts, Chronoamperometric measurements at 0.5 V (vs. RHE) in O_2-saturated 0.1 M KOH electrolyte were

applied to evaluate the stability of CoS_2-Co/NC, Co/NC and commercial 10 wt. % Pt/C catalysts. As exhibited in Fig. 7d, the current-time (i-t) chronoamperometric response for CoS_2-Co/NC electrode exhibits an extremely slow attenuation with a high retention of ~ 98% after 10 h, whereas the electrodes prepared by Co/NC or commercial 10 wt. % Pt/C catalysts show fast current loss under the same conditions. The high ORR activity and greatly enhanced ORR stability of CoS_2-Co/NC nanocomposites are related to their unique nanostructures, in which Co-N-C acts as high-efficient electrocatalytic active sites, and CoS_2 shells prevent the highly active Co-N-C from deactivation. The superior ORR performances of CoS_2-Co/NC nanocomposites strongly demonstrate the great importance of constructing catalysts with rationally designed structure and composition.

4. CONCLUSIONS

In summary, a new type of non-precious metal catalyst based on CoS_2-Co nanoparticles loaded on N-doped porous carbon nanostructures (CoS_2-Co/NC) has been synthesized by the carbonization of MOFs with a consequent sulfuration process. These nanocomposites are comprised of inner Co and outer CoS_2 shells. As an electrocatalyst for ORR, the CoS_2-Co/NC nanostructures exhibit remarkable electrocatalytic activity and durability towards ORR, due to their unique structural merits, including highly effective Co-N-C active sites, porous carbon nanostructures for rapid mass transfer, and CoS_2 protective layers that prevent Co-N-C active sites from deactivation.

References

1. G. Wu, P. Zelenay, *Acc. Chem. Res.*, 46 (2013) 1878.
2. Y. Nie, L. Li and Z. Wei, *Chem. Soc. Rev.*, 44 (2015) 2168.
3. J. Zhang, Z. Zhao, Z. Xia and L. Dai, *Nat. Nanotech.*, 10 (2015) 444.
4. F. Jaouen, E. Proietti, M. Lefèvre, R. Chenitz, J.-P. Dodelet, G. Wu, H. T. Chung, C. M. Johnston and P. Zelenay, *Energy Environ. Sci.*, 4 (2011) 114.
5. C. Cui, L. Gan, M. Heggen, S. Rudi and P. Strasser, *Nat. Mater.*, 12 (2013) 765.
6. J. C. Meier, C. Galeano, I. Katsounaros, A. A. Topalov, A. Kostka, F. Schüth and K. J. Mayrhofer, *ACS Catal.*, 2 (2012) 832.
7. H. Peng, Z. Mo, S. Liao, H. Liang, L. Yang, F. Luo, H. Song, Y. Zhong and B. Zhang, *Sci. Rep.*, 3 (2013) DOI: 10.1038/srep01765.
8. Z. Y. Wu, X. X. Xu, B. C. Hu, H. W. Liang, Y. Lin, L. F. Chen and S. H. Yu, *Angew. Chem. -Int. Edit.*, 54 (2015) 8179.
9. L. Shang, H. Yu, X. Huang, T. Bian, R. Shi, Y. Zhao, G. I. Waterhouse, L. Z. Wu, C. H. Tung and T. Zhang, *Adv. Mater.*, 28 (2015) 1668.

10. Y. Liang, Y. Li, H. Wang, J. Zhou, J. Wang, T. Regier and H. Dai, *Nat. Mater.*, 10 (2011) 780.
11. Y. Liang, Y. Li, H. Wang and H. Dai, *J. Am. Chem. Soc.*, 135 (2013) 2013.
12. N. Mahmood, C. Zhang, J. Jiang, F. Liu and Y. Hou, *Chem.-A Eur. J.,* 19 (2013) 5183.
13. K. Gong, F. Du, Z. Xia, M. Durstock and L. Dai, *Science*, 323 (2009) 760.
14. J. Liang, Y. Jiao, M. Jaroniec and S. Z. Qiao, *Angew. Chem. -Int. Edit.*, 51 (2012) 11496.
15. H. X. Zhong, J. Wang, Y. W. Zhang, W. L. Xu, W. Xing, D. Xu, Y. F. Zhang and X. B. Zhang, *Angew. Chem. -Int. Edit.*, 53 (2014) 14235.
16. W. Ai, Z. Luo, J. Jiang, J. Zhu, Z. Du, Z. Fan, L. Xie, H. Zhang, W. Huang and T. Yu, *Adv. Mater.*, 26 (2014) 6186.
17. M. Graglia, J. Pampel, T. Hantke, T. P. Fellinger and D. Esposito, *ACS Nano*, 10 (2016) 4364.
18. Z. Chen, D. Higgins, A. Yu, L. Zhang and J. Zhang, *Energy Environ. Sci.*, 4 (2011) 3167.
19. G. Wu, K. L. More, C. M. Johnston and P. Zelenay, *Science*, 332 (2011) 443.
20. G. Nam, J. Park, S. T. Kim, D.-b. Shin, N. Park, Y. Kim, J.-S. Lee and J. Cho, *Nano lett.*, 14 (2014) 1870.
21. S. Gadipelli, T. Zhao, S. A. Shevlin and Z. Guo, *Energy Environ. Sci.*, 9 (2016) 1661.
22. W. Xia, R. Zou, L. An, D. Xia and S. Guo, *Energy Environ. Sci.*, 8 (2015) 568.
23. H. Hu, L. Han, M. Yu, Z. Wang and X. W. D. Lou, *Energy Environ. Sci.*, 9 (2016) 107.
24. X. Zhang, R. Liu, Y. Zang, G. Liu, G. Wang, Y. Zhang, H. Zhang and H. Zhao, *Chem. Comm.*, 52 (2016) 5946.
25. R. Zhang, S. He, Y. Lu and W. Chen, *J. Mater. Chem.* A, 3 (2015) 3559.